Analysis of an Electrostatically Actuated MEMS Drop Ejector

E. P. Furlani[1] and M. C. Carter[2]

[1]Eastman Kodak Company, Kodak Research Laboratories
1999 Lake Avenue, Rochester, New York 14650-2216
edward.furlani@kodak.com

[2]Flow Science Inc., Santa Fe, New Mexico 87505

ABSTRACT

We present an analysis of an electrostatic-based MEMS drop ejector. The ejector consists of a microfluidic chamber with a piston that is suspended a few micrometers beneath a nozzle plate. A drop is ejected when the piston is electrostatically driven toward the orifice. We discuss the operating physics of the ejector, and present a lumped-element model for predicting its performance. We compare the analytical predictions with CFD analysis.

Keywords: Microfluidics, MEMS, squeeze film analysis, microdrop ejection, drop-on-demand.

1 INTRODUCTION

MEMS are finding increasing use for applications that require the controlled generation and delivery of picoliter-sized droplets. Common applications include biomedical and biochemical microdispensing and most notably, inkjet printing. The most common MEMS drop ejectors operate in a drop-on-demand (DOD) mode. In DOD devices, micro-droplets are produced as needed by generating a sharp, short-lived pressure pulse within a microfluidic chamber beneath an orifice plate. The pressure profile is tuned to eject a droplet with a desired volume and velocity. The most common methods for producing the drop ejection pressure involve piezoelectric actuation or the generation of a thermally induced vapor bubble (bubble-jet). In this presentation we discuss an alternative method of drop generation that is based on electrostatic actuation. Specifically, we study a MEMS drop ejector that consists of a microfluidic chamber with a piston that is suspended a few micrometers beneath and orifice plate (Fig. 1). The piston is supported by cantilevered polysilicon flexure members that act as restoring springs when the piston is displaced from its equilibrium position (Fig. 1a). To eject a drop, a potential difference is applied between the orifice plate and the piston, and this produces an electrostatic force that moves the piston toward the orifice. The moving piston generates a squeeze-film pressure distribution in the gap region above it that acts to eject the drop (Fig. 2). Specifically, a peak pressure (stagnation pressure) obtains at a specific radius (stagnation radius), which is greater than the orifice radius. Thus, the fluid within the stagnation radius is confined, and forced through the nozzle as the piston moves toward it. A portion of this fluid ultimately detaches from the ejector and forms into a droplet; the remainder retracts back into the ejector as the piston returns to its equilibrium position. A drop ejector based on this principle has been fabricated and characterized at Sandia National Laboratories (Fig. 1) [1,2].

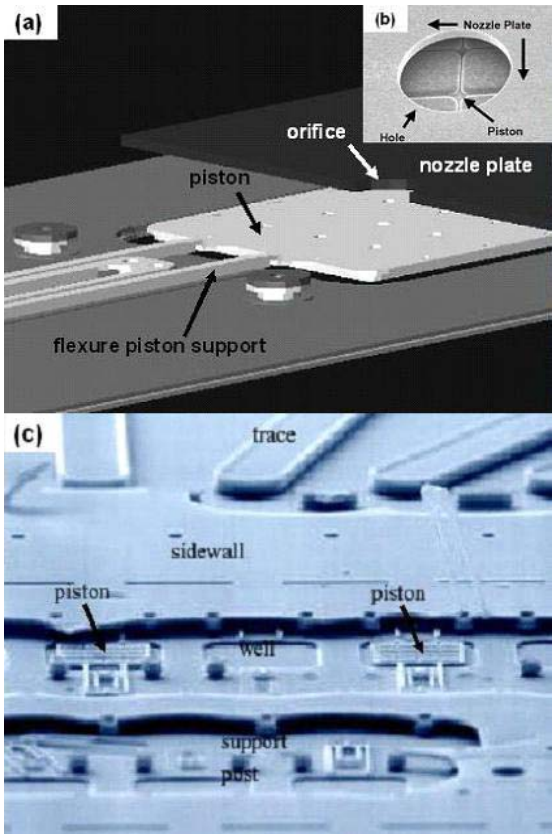

Figure 1: MEMS drop ejector (adapted from reference [1]): (a) schematic showing cantilevered piston and cut away view of nozzle plate; (b) close-up view of orifice and piston, and (c) SEM of ejectors (cover removed).

In this paper, we discuss the basic operating physics of the ejector, and we present an analytical lumped-element model for predicting its performance. We use the model to study device performance. We compare the analytical predictions with CFD analysis that takes into account the coupled piston-fluid interactions.

2 ANALYTICAL MODEL

We model the drop ejector using a lumped-element axisymmetric analysis (Fig. 2). The motion of the piston is obtained from the equation for the force balance on the piston

$$\left(m_p + m_{eff}(t)\right)\frac{dv_p}{dt} = F_a(t) - kx_p(t) - 2\pi\int_0^{r_p} p(r, v_p, t)\, r\, dr + \sum F_f \tag{1}$$

where m_p, $x_p(t)$, and $v_p(t)$ are the mass, position, and velocity of the piston, $m_{eff}(t)$ is the effective mass of the fluid that it accelerates, $F_a(t)$ is the applied electrostatic force, k is a spring constant for the polysilicon support members, and $p(r, v_p, t)$ is the squeeze-film pressure distribution that develops between the piston and the nozzle, which acts to resist the piston motion. The term $\sum F_f$ represents other forces due to the fluid motion.

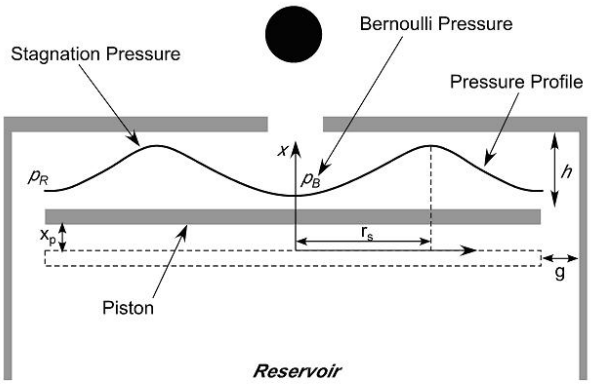

Figure 2: Axisymmetric model of MEMS drop ejector.

2.1 Stagnation Pressure

The pressure distribution $p(r, v_p, t)$ developed by the moving piston is obtained by applying Reynolds lubrication theory to the axisymmetric geometry shown in Fig. 2. The pressure above the piston satisfies the following equation

$$\frac{1}{r}\frac{\partial}{\partial r}\left(r\frac{\partial p(r,t)}{\partial r}\right) = -\frac{12\mu}{h^3(t)}v_p(t) \qquad (r_0 \le r \le r_p) \tag{2}$$

where μ is the fluid viscosity, v_p is the piston velocity, r_o and r_p are the radius of the orifice and the piston, respectively, and $h(t)$ is the distance from the piston to the nozzle plate. The general solution to this equation is of the form

$$p(r,t) = -\frac{3\mu v_p(t)}{h^3}r^2 + c_1\ln(r) + c_2, \tag{3}$$

where c_1 and c_2 are constants determined from boundary conditions [2]. The pressure distribution (3) peaks at a value p_s (stagnation pressure) at the stagnation radius $r_s(t)$,

$$r_s(t) = \sqrt{\frac{h^3 c_1}{6\mu v_p(t)}}, \tag{4}$$

as shown in Fig. 2. We assume that fluid above the piston and within the stagnation radius ($r \le r_s(t)$) flows toward the orifice, while fluid beyond this point ($r > r_s(t)$) flows into the reservoir. The boundary conditions for this problem are

$$\begin{aligned} p(r,t) &= p_B(t) \qquad (r = r_o) \\ p(r,t) &= p_R(t) \qquad (r = r_p) \end{aligned} \tag{5}$$

where $p_B(t)$ and $p_R(t)$ are the pressures beneath the orifice $(r \le r_o)$, and at the edge of the piston, respectively, which are related to the flow rates at those points. Analytical expression for $p(r,t)$, $r_s(t)$, $p_B(t)$, and $p_R(t)$ can be found in the literature [2].

2.2 Effective Mass

We take into account inertial effects by estimating the mass of fluid accelerated by the piston as it moves. As above, we assume that the fluid within the stagnation radius flows toward the orifice, while the fluid beyond this point flows through the gap into the reservoir. From our analysis we find that the total effective mass of the fluid is [2]

$$m_{eff}(t) = \rho\pi\left[\frac{r_p^3 + r_0^3 + 4r_s^3}{3} - r_s^2\left(r_p + r_0\right)\right] + \rho\pi l_0 r_s^2(t) + \rho\pi l_0 r_s^2(t) + \rho\pi l_p\left(r_p^2 - r_s^2(t)\right) \tag{6}$$

NSTI-Nanotech 2009, www.nsti.org, ISBN 978-1-4398-1784-1 Vol. 3, 2009

2.3 Equation of Motion

The equation of motion, Eq. (1), contains an expression $\sum F_f$ that accounts for additional forces due to fluid flow. Two such forces arise from the flow across the top surface of the orifice, and boundary of the gap at the reservoir. These additional forces have the form,

$$F_o(t) = \rho\pi r_o^{\,2} v_o^{\,2}(t)\,, \tag{7}$$

and

$$F_g(t) = \rho 2\pi r_p g\, v_g^{\,2}(t)\,, \tag{8}$$

where $v_g(t)$ is the average velocity across the gap/reservoir interface. We collect all of the relevant terms and obtain the following equation of motion for the piston

$$\begin{aligned}\left(m_p + m_{eff}(t)\right)\frac{dv_p}{dt} &= F_a(t) - kx_p(t) - \pi r_o^2 p_B(v_p,t) \\ &- 2\pi\int_{r_o}^{r_p} p(r,v_p,t)\,r\,dr - \rho\frac{\pi^2\left(r_p^{\,2}-r_s^{\,2}\right)^2}{\left(2\pi r_p g\right)}v_p^{\,2}(t) - \rho\pi\frac{r_s^4}{r_o^2}v_p^{\,2}(t) \\ &- \rho\pi\left[\frac{r_p^{\,3}+r_0^{\,3}+4r_s^{\,3}}{3} - r_s^{\,2}\left(r_p+r_0\right)\right]\frac{v_p^{\,2}(t)}{\left(h_0 - x_p(t)\right)}\end{aligned} \tag{9}$$

To perform device simulation, we integrate this nonlinear ODE using a fourth-order Runge-Kutta method.

3 RESULTS

We use Eq. (9) to study the behavior of the drop ejector. We solve for the piston velocity and use this to obtain the average velocity $v_o(t)$ and volume flow rate $Q_o(t)$ of the fluid ejected through the nozzle,

$$v_o(t) = \frac{r_s^{\,2}(t)v_p(t)}{r_o^{\,2}}\,, \tag{10}$$

and

$$Q_o(t) = \pi r_s^{\,2}(t)v_p(t)\,. \tag{11}$$

It is important to note that this analysis does not take into account the complex free-surface dynamics that govern the fluid-nozzle interaction and the ultimate formation of the drop, i.e., pinch-off, satellites, etc. To compensate for this, we estimate the actual observed flow rate $Q_{exp}(t) = \beta Q_o(t)$ using a fitting parameter β, which we determine using CFD analysis. Once determined, this parameter is fixed for all of the analysis. We also track the total volume of fluid V_{eject} ejected during actuation by integrating the flow rate through the orifice during the applied force,

$$V_{eject} = \int_0^{\tau} Q_{exp}(t)\,dt\,, \tag{12}$$

where τ is the duration of the applied voltage or E field.

We apply the model to an ejector with an orifice radius r_o=10 μm. The piston is polysilicon with a thickness of 2 μm. The reservoir gap is g = 10 μm, and the fluid is water. We study the ejection process using a constant electric field and no spring-restoring force (k = 0). The applied field is E = 25 V/μm and the activation period is $\tau = 4.4\mu s$. During this time, the applied electrostatic force on the piston is $F_a(t) = \varepsilon\pi\left(r_p^{\,2} - r_o^{\,2}\right)E^2/2$ where $\varepsilon = 70\varepsilon_0$.

We track the piston velocity, flow rate through the orifice, and ejected volume. We perform a parametric analysis where we vary the piston radius r_p = 50, 60, and 70 μm. For each radius, we evaluate ejection performance for three different initial piston-to-nozzle distances h_0 = 3.5, 4.0, and 4.5 μm. We calibrate our analytical model using CFD analysis that takes into account fluid-structure coupling, i.e., the displacement of the piston depends upon the applied electrostatic force, and the resistance to motion due to pressure in the fluid.

We use the FLOW-3D software for the CFD, which is a volume-of-fluid (VOF)-based solver. From our CFD analysis we determine a fitting parameter β = 0.75, i.e., the analytical model overpredicts the ejected volume by 25% compared to the CFD analysis. This is expected as the model does not take into account several effects that tend to lower the ejected volume including the back pressure at the orifice due to the developing meniscus, etc. We use the same value of β for all of our analysis. The analytical and CFD predictions of ejected fluid volume are compared in Table 1. A typical analytical calculation required only a few seconds to complete, while the fully coupled CFD required 55 min to simulate 4.4 μs of the ejection process.

	$Q_{Analytical}/Q_{CFD}$ (pl)		
	R_p (μm)		
	50	60	70
h_0 (μm)			
3.5	4.13/4.4	4.93/5.2	5.67/5.6
4.0	4.79/5.0	5.7/5.7	6.64/6.35
4.5	5.27/5.54	6.4/6.35	7.48/7.05

Table 1: Comparison of total volume ejected through the orifice during the ejection period 4.4 μs.

Next we compare the piston displacement, flow rate through the orifice, and ejected volume ($0 \le t \le \tau$) for the 140 μm piston with an initial position 3.5 μm beneath the nozzle. These are shown in Figs. 3, 4, and 5, respectively.

Note that the analytical model tends to overpredict the piston displacement and orifice flow rate during the initial stage of ejection, and underpredict these variables during the latter stage. A CFD analysis of drop ejection for the 140 µm piston with h_0 = 3.5 µm is shown in Fig. 6. The final ejected drop volumes and velocities from the CFD analysis are given in Table 2. Only the primary drop volumes are recorded, i.e., satellite drops are not included.

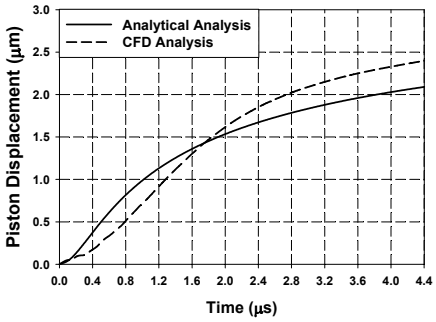

Figure3: Piston displacement (R_p = 70 µm, h_0 = 3.5 µm).

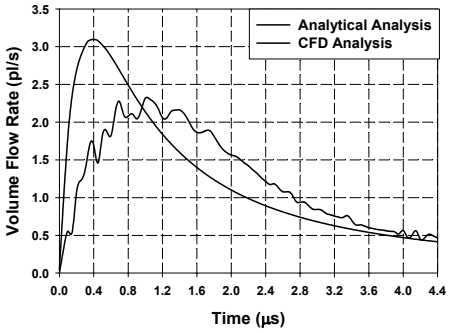

Figure 4: Orifice flow rate (R_p = 70 µm, h_0 = 3.5 µm).

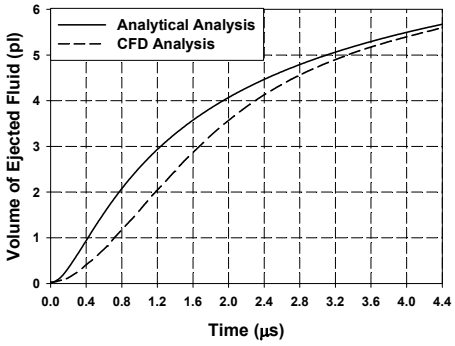

Figure 5: Ejected volume (R_p = 70 µm, h_0 = 3.5 µm).

4 CONCLUSIONS

We have presented a lumped-element model for predicting the performance of the squeeze-film-dominated electrostatic ejector shown in Fig. 1. The model needs to be calibrated using a limited number of CFD simulations in order to provide more accurate estimates of the orifice flow rate and total ejected volume of fluid. Once calibrated, the model enables rapid parametric analysis of performance as a function of key device parameters including the piston size, orifice diameter, and initial gap beneath the nozzle.

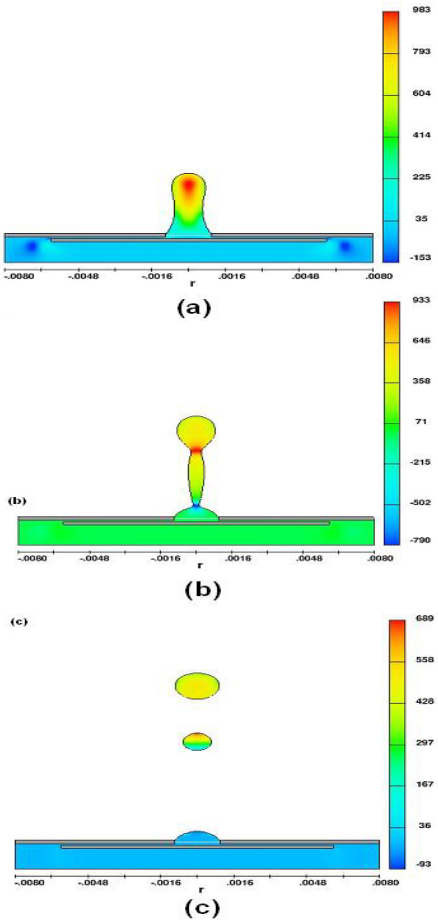

Figure 6: CFD simulation of drop ejection: (a) t = 4.4 µs, (b) t = 10 µs, and (c) t = 20 µs.

Drop Volume (pl)/DropVelocity (m/s)			
	R_p (µm)		
	50	60	70
h_0 (µm)			
3.5	3.0/0.86	3.7/2.0	3.13/4.40
4.0	3.56/2.1	4.78/3.24	3.78/5.54
4.5	4.0/3.12	4.95/3.8	4.35/6.6

Table 2: CFD drop volumes and velocities.

REFERENCES

[1] A. Gooray, G. Roller, P. Galambos, K. Zavadll, R. Givler, F. Peter, and J. Crowley, J. of Imaging Science and Technology, **46**, No. 5, 415-432, 2002.
[2] E. P. Furlani, J. Phys. D: Appl. Phys., **37**, 2483-2488, 2004.